PLOS ONE

Targeting the somatosensory system with AAV9 and AAV2retro viral vectors

Alexander G. J. Skorput[1¤], Reshma Gore[1], Rachel Schorn[1], Maureen S. Riedl[1], Ezequiel Marron Fernandez de Velasco[2], Bailey Hadlich[1], Kelley F. Kitto[1], Carolyn A. Fairbanks[1,2,3], Lucy Vulchanova[1]*

1 Department of Neuroscience, Medical School, University of Minnesota, Minneapolis, Minnesota, United States of America, **2** Department of Pharmacology, Medical School, University of Minnesota, Minneapolis, Minnesota, United States of America, **3** Department of Pharmaceutics, College of Pharmacy, University of Minnesota, Minneapolis, Minnesota, United States of America

¤ Current address: Department of Molecular and System Biology, Geisel School of Medicine at Dartmouth, Lebanon, NH, United States of America
* vulch001@umn.edu

Abstract

Adeno-associated viral (AAV) vectors allow for site-specific and time-dependent genetic manipulation of neurons. However, for successful implementation of AAV vectors, major consideration must be given to the selection of viral serotype and route of delivery for efficient gene transfer into the cell type being investigated. Here we compare the transduction pattern of neurons in the somatosensory system following injection of AAV9 or AAV2retro in the parabrachial complex of the midbrain, the spinal cord dorsal horn, the intrathecal space, and the colon. Transduction was evaluated based on Cre-dependent expression of tdTomato in transgenic reporter mice, following delivery of AAV9 or AAV2retro carrying identical constructs that drive the expression of Cre/GFP. The pattern of distribution of tdTomato expression indicated notable differences in the access of the two AAV serotypes to primary afferent neurons via peripheral delivery in the colon and to spinal projections neurons via intracranial delivery within the parabrachial complex. Additionally, our results highlight the superior sensitivity of detection of neuronal transduction based on reporter expression relative to expression of viral products.

Introduction

AAV vectors have been used for transgene delivery to different components of the nociceptive system in rodents for nearly two decades. Transduction of primary afferent neurons has been demonstrated using intrathecal [1, 2], intraganglionic [3–5], intraneural [6, 7], or peripheral [8, 9] injections. Intraspinal AAV vector delivery has substantially aided neuroanatomical and functional investigations of dorsal horn circuits (for example, [10–12]). In addition, intraparenchymal AAV injections within various brain nuclei have been employed in mapping of supraspinal circuits involved in pain processing [13–16].

AAV serotypes vary in their transduction efficiency via different routes of administration. A number of serotypes have been characterized for intraganglionic, intraspinal, intrathecal,

and to a lesser degree peripheral delivery [7, 17, 18]. Among these, AAV9 is distinguished by its efficient transduction of DRG neurons following intrathecal delivery [1] and its capacity for neuronal transduction following localized peripheral delivery [19]. AAV serotypes also differ in their ability to enter neurons via their axon terminals and undergo retrograde transport to the cell body, a property that is particularly useful for targeting of projection neurons in the central nervous system [20]. AAV2retro is a recombinant virus that was specifically engineered for retrograde neuronal transduction [21], and its use has contributed extensively to mapping of neural circuits (for example, see [15, 22–25]).

The main objective of this study was to explore AAV2retro-mediated gene transfer within the somatosensory system and compare it to that mediated by AAV9. In addition to the widely used intrathecal and intraspinal routes of delivery, we characterized transduction of spinal projection neurons via viral delivery of AAV9 and AAV2retro to the parabrachial nuclear complex. We further employed intracolonic AAV9 and AAV2retro injections to evaluate the potential for selective gene transfer to DRG neurons based on site-specific peripheral viral vector delivery. Neuronal transduction by AAV9 or AAV2retro, driving the expression of a fusion Cre/GFP protein, was evaluated based on Cre-dependent expression of tdTomato in transgenic reporter mice. Although we did not conduct direct quantitative comparisons between the two serotypes due to differences in the viral preparations, our observations indicate differences in the access of AAV9 and AAV2retro to neurons of the somatosensory system that will inform future applications of these vectors.

Methods

Animals

All procedures were performed in accordance with the National Institutes of Health *Guide for the Care and Use of Laboratory Animals* and approved by the University of Minnesota Institutional Animal Care and Use Committee. Experiments were performed in male and female transgenic mice harboring a flox-stop-tdTomato reporter gene (Ai14 mice; jax# 007914) and in wild type C57/Bl6 mice. Both heterozygous and homozygous Ai14 were used in this study, but comparisons between vectors were made within the same genotype. Further, we have noted no differences in the fluorescence intensity of individual tdTomato expressing neurons of heterozygous and homozygous Ai14 mice following viral Cre-mediated recombination, likely due to the weeks long time period between transduction and tissue harvest resulting in a near maximal intracellular load of tdTomato. Mice were 4–10 weeks old at the time of viral injections. For each route of viral vector administration, mice treated with AAV9 or AAV2retro were age-matched. Survival time post-administration was dictated for each route by estimates of the time required for retrograde transport, viral expression, and expression of the reporter gene.

Viral vectors

AAV2retro.*hSyn*.Cre-eGFP, abbreviated as AAV2retro was packaged by the Viral Vector and Cloning Core (VVCC) at the University of Minnesota. AAV9.*hSyn*.Cre-eGFP, abbreviated as AAV9, was packaged by the VVCC or obtained from the University of Pennsylvania Vector Core (see below for titer information). Our AAV2retro and AAV9 viral preparations were not produced in parallel, and thus were not titer-matched. Titer-matching would have required dilution of one of the preps. Dilution of viral preparations could result in uneven distribution of viral particle aggregates or compromise their integrity and/or infectivity due to shear forces that occur during pipetting. AAV9 and AAV2retro contained the same construct (addgene plasmid #105540, courtesy of Dr. James Wilson), which encodes a Cre/GFP fusion protein

under control of the human synapsin promoter. Thus, viral transduction leads to Cre-mediated recombination and tdTomato expression in transduced neurons of Ai14 mice.

Parabrachial nucleus injections

Mice were mounted in a stereotaxic frame (Stoelting, 51600, Wood Dale, IL) under isoflurane anesthesia (2.5–4%) and injected with 500 nL of AAV9 ($3x10^{13}$ GC/mL, VVCC), AAV2retro ($2.5x10^{14}$GC/mL, VVCC), or Fast-DiI (2.5 mg/ml in dimethylformamide; ThermoFisher, Waltham, MA). A pulled borosilicate glass pipette with a tip diameter of ~20 µm was attached to a picospritzer (Parker Hannifin, Hollis, NH) and a microsyringe (Hamilton, Reno, NV) by way of a three-way stopcock and the dead space was filled with mineral oil. The pipette was attached to a stereotaxic manipulator (Stoelting) and the tip was advanced 3 mm ventral from the level of the meninges through a small burr hole in the skull positioned 1.5 mm left of midline at a location 0.5 mm caudal from true lambda. The injectate was delivered under pressure, the pipette was slowly removed from the brain after a 5min rest period, and the skin was closed with VetBond (3M, St,Paul, MN). Animals were allowed to recover on a heated pad, and meloxicam (2 mg/kg, s.c.) was given for post-operative analgesia for 3 consecutive days. Tissues were collected for analysis 6 (AAV) or 4 (DiI) weeks after injections.

Intraspinal injections

As in previous studies [10, 11], intraspinal injections were delivered at the L3-L4 levels of the mouse spinal cord, where sensory inputs from the hindpaws are processed. Mice were anesthetized with a mixture of ketamine/xylazine/acepromazine (75mg/kg ketamine, 5mg/kg xylazine, 1 mg/kg acepromazine, i.p.). The back skin of anesthetized animals was incised and the soft tissue overlying the L3-L4 spinal cord segments was blunt dissected to the level of the vertebral laminae. The ligament between the T12 and T13 laminae and the underlying dura mater were parted and the right dorsal horn was injected with 1 µL of AAV9 ($3x10^{13}$ GC/mL, VVCC, n = 3; $8.5x10^{13}$ GC/mL, VVCC, n = 3), or AAV2retro ($2.5x10^{14}$GC/mL, VVCC; n = 4), at a depth of 300 µm using the same pressurized pipette setup as for PBN injection. The muscles and subcutaneous layers were then reapproximated and closed with surgical suture (4–0 monocryl with PC-5 needle), and the skin was closed with surgical staples. Animals were allowed to recover on a heated pad and meloxicam (2 mg/kg, s.c.) was given for post-operative analgesia for 3 consecutive days. Tissues were collected for analysis 2 weeks after injections.

Intrathecal injections

AAV9 ($8.5x10^{13}$ GC/mL, VVCC) or AAV2retro ($1x10^{13}$GC/mL, VVCC) were delivered intrathecally (i.t.) by direct lumbar puncture in conscious adult mice as described [26, 27]. The mice were gently gripped by the iliac crest, and a 30-gauge, 0.5-inch needle connected to a 50 µL Luer-hub Hamilton syringe was used to deliver 10 µL of injectate into the subarachnoid space over 1-3s at the level of the cauda equina between the L5/L6 vertebrae. The duration of the procedure was approximately 15–30 s per mouse. All injections were confirmed by observation of a tail flick upon entry into the intrathecal space. Tissues were collected for analysis 3 weeks after injections.

Intracolonic injections

Intracolonic injections were performed as previously described [28], in two cohorts of Ai14 mice: cohort 1 received AAV9 ($2.7x10^{13}$ GC/mL, UPenn Viral Core; n = 3) or AAV2retro ($2.5x10^{14}$GC/mL, VVCC; n = 3); cohort 2 received AAV9 ($8.5x10^{13}$ GC/mL, VVCC; n = 5) or

AAV2retro ($1x10^{13}$GC/mL, VVCC; n = 6). Based on tdTomato labeling in the DRG, the injection success rate for cohort 1 was 100% and for cohort 2 ~50%. In addition, three C57/Bl6 mice were injected with the AAV9 vector. Animals were anesthetized using isoflurane (2.5–4%). A vertical incision (~ 3 cm) was made in the lower abdomen of adult mice, and the descending colon was exposed. Mice received a single 4-µl injection of viral vector. Injections were made into the wall of the descending colon horizontal to the longitudinal axis of the colon, using a 10-µl Hamilton syringe attached to a 30-gauge needle. The needle was left in place for 1 minute to prevent reflux. Following injection, the abdominal wall was sutured (Ethicon Cat# Z304H), and the overlying skin was closed with Vetbond. Mice were allowed to recover on a heated pad and meloxicam (2 mg/kg, s.c.) was given for post-operative analgesia for 3 consecutive days. Tissues were collected for analysis 3–4 weeks after injections.

Immunohistochemistry

Mice were deeply anaesthetized with isoflurane and perfused via the heart with calcium-free Tyrode's solution (in mM: NaCl 116, KCl 5.4, $MgCl_2 \cdot 6H_20$ 1.6, $MgSO_4 \cdot 7H_2O$ 0.4, NaH_2PO_4 1.4, glucose 5.6, and $NaHCO_3$ 26) followed by fixative (4% paraformaldehyde and 0.2% picric acid in 0.1M phosphate buffer pH 6.9 or 4% paraformaldehyde in phosphate buffered saline). Tissues were dissected and incubated in 10% sucrose (in PBS) solution overnight. Tissues were then cryostat-sectioned at 14–30µm, and the sections were mounted onto gel-coated slides and stored at -20˚ C until use. Sections were thawed and incubated in diluent (PBS with 0.3% Triton-X100; 1% BSA, 1% normal donkey serum) for 1h at room temperature followed by incubation in primary antibodies (rabbit anti Ds-red, Takara, cat# 632496, 1:1000; or chicken anti-GFP; Abcam, cat# ab113970, 1:1000) overnight at 4˚C. Sections were rinsed in PBS (3X10 min each), incubated in species-appropriate secondary antibodies (Cy3-conjugated donkey anti-rabbit, 1:300, cat# 711-165-152, and Alexa488-conjugated donkey anti-chicken, 1:100, cat# 703-545-155, Jackson ImmunoResearch, West Grove, CA) for 1h at room temperature, rinsed again using PBS, and coverslipped using glycerol and PBS containing p-phenylenediamine (Sigma). The specificity of the antisera was confirmed by lack of labeling in the absence of viral injections. Following incubation in primary and secondary antibodies, some DRG sections were stained in NeuroTrace (1:1000, Invitrogen). For visualization of Fast-DiI, tissue sections were rehydrated in diluent for 30 min and coverslipped.

Imaging

Images were acquired in an Olympus BX2 microscope equipped with a Fluoview 1000 scan head, software version 4.1.5.5; objectives—UPLAPO 4x/0.16 NA (Fig 1C1), UPLSAPO 20x/0.85 NA (Fig 1A2, 1B2 and 1C2; Fig 4D–4F), UPLAPO 10x/0.4 NA (Figs 2 and 3, Fig 4A2 and 4B2); confocal aperture was set to software-determined auto settings. Single or sequential multi-fluorescent images were collected using 405 nm (NeuroTrace), 488 nm (Alexa488), and 543 nm (Cy3 or DiI) laser excitation and collecting emission between 425–475 nm, 505–525 nm, and 550–650 nm, respectively. Images we also collected with a Nikon FN1 upright stand equipped with an A1R HD MP laser scanning head and a motorized Prior stage and piezo Z drive (for sample positioning and focus) and controlled with NIS Elements 5.1 software; objectives—Nikon Plan Fluor DIC 10x/0.3NA (Fig 1A1, 1B1 and 1F; pinhole 12.77 µm, confocal mode, excitation 561 nm, emission 575–625 nm; tiled 4x4 acquisition for A1 and B1) and Nikon Plan Apo LWD 25x water-immersion/NA 1.1 (Fig 4A1 and 4B1; multiphoton mode, Mai Tai DeepSee 920 nm excitation, 570–640 nm emission, GaAsP NDD). For optimal visualization, the representative images used in the figures were adjusted for brightness, contrast, and
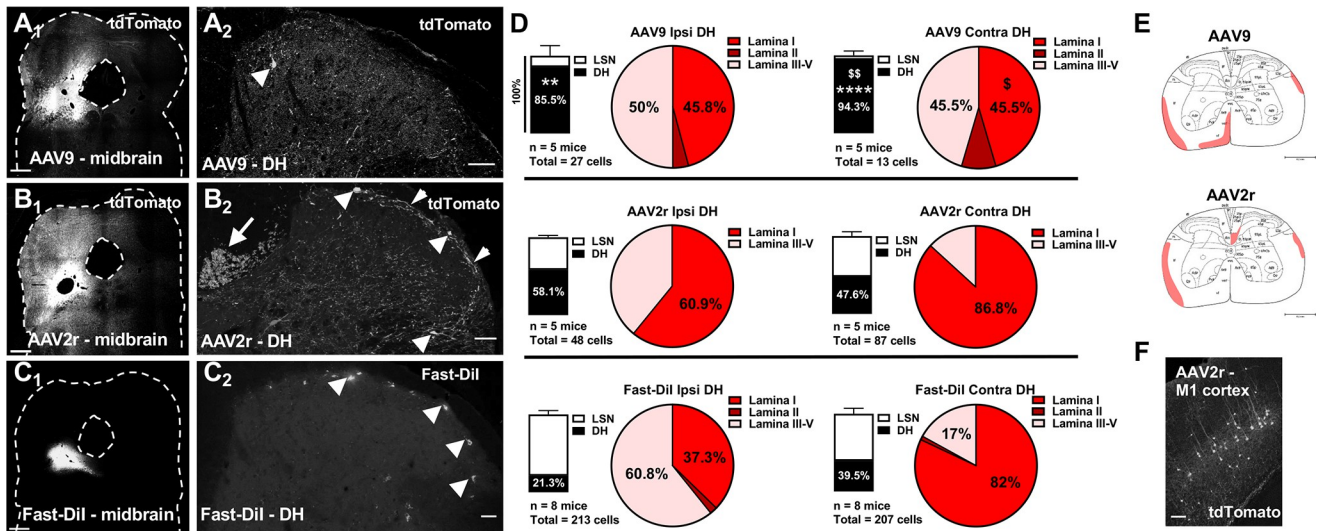
Fig 1. Targeting of spinoparabrachial neurons by AAV9, AAV2retro, and DiI. A-C, Representative images of the parabrachial complex (A1, B1, C1; scale bars = 500 μm) and dorsal spinal cord (A2, B2, C2; scale bars = 50 μm) following parabrachial complex injections of AAV9 (A), AAV2retro (AAV2r, B), or Fast-DiI (C). The images in B2 and C2 represent a maximum intensity projection of 3D stacks spanning 12 and 16 μm, respectively, and collected with a 4-μm z-step. Arrowheads in A2, B2 and C2 highlight labeled spinal projection neurons in the superficial dorsal horn. Additionally, in B2, the short arrow highlights a plexus of labeled processes in lamina I, and the long arrow indicates labeling of the dorsal corticospinal tract. **D,** Stacked Bars represent the relative distribution of labeled projection neurons between the dorsal horn (DH) and the lateral spinal nucleus (LSN) in the ipsilateral (left) and contralateral (right) spinal cord following injection with AAV9 (top), AAV2retro (middle), or Fast-DiI (bottom) (** p<0.01, **** p<0.0001, compared to Fast-DiI; $ $ p<0.01, compared to AAV2r). The total number of labeled neurons analyzed and the number of animals (n) is noted under the stacked bars. Pie charts in D show the percentage of labeled neurons present in lamina I-V of DH. Proportions of labeled neurons in spinal laminae were compared using Two-way ANOVA and Bonferroni posttest ($, p<0.05 compared to AAV2r). **E,** The average labeling of spinal tracts at the level of L3 is shaded for AAV9 (E1) and AAV2r (E2). **F,** Retrograde labeling of cortical neurons in primary motor cortex (M1) following parabrachial injection of AAV2retro; scale bar = 150μm.

https://doi.org/10.1371/journal.pone.0264938.g001

color using Adobe Photoshop software. Non-linear adjustment was applied simultaneously to images from the same experiment.

Quantitative analysis of spinal projection neurons

Spinal neurons labeled by parabrachial injections in the rostral lumbar enlargement (L1-L3) were counted manually and mapped by an observer blinded to the treatments under wide field epifluorescence in eighteen 30-μm immunostained tissue sections separated by 120 μm. Brains were sectioned coronally at 30μm and sections were immunostained and assessed for tdTomato immunolabeling by a blinded observer at intervals of 600 μm.

Quantitative analysis of DRG neurons after intrathecal delivery

Different approaches for quantitative analysis of transduction in DRG neurons were applied for intrathecal and intracolonic AAV delivery to allow comparisons with previous literature. For intrathecal AAV delivery, DRG sections were immunolabeled and counterstained with NeuroTrace (1:1000, Invitrogen). Confocal images were collected with the Olympus Fluoview system as described above (UPLAPO 10x/0.4 NA), using uniform imaging parameters that avoided saturation. Image analysis was performed by trained observers blinded to the experimental groups using Fiji. NeuroTrace-labeled neuronal profiles with nuclei were outlined in 5 evenly spaced sections per DRG, and measurements of the area and the mean grey value of tdTomato immunoreactivity in each profile were obtained. To estimate the proportion of
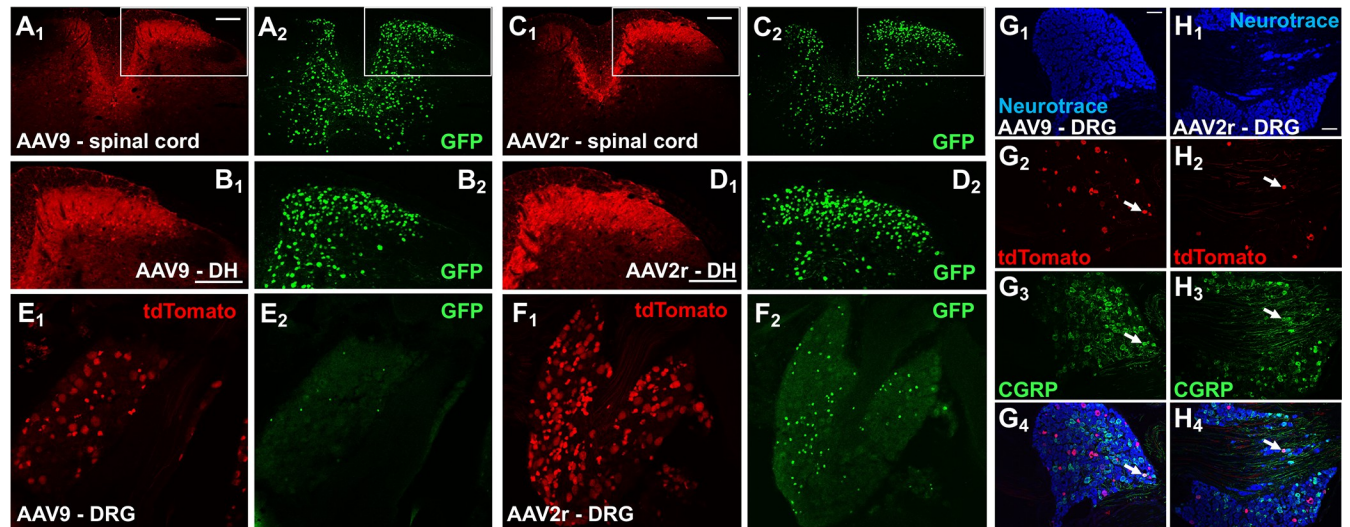
Fig 2. Intraspinal delivery of AAV9 and AAV2retro viral vectors leads to effective transduction of both spinal and primary afferent neurons. A-D, tdTomato (red, subscript 1) and GFP (green, subscript 2) immunofluorescence in Ai14 mice injected unilaterally in the L3/L4 region of spinal cord with AAV9 (A and B), or AAV2retro (C and D); scale bars = 150 μm. The discrepancy in the tdTomato and GFP labeling is largely due to the differential subcellular localization of the two reporter proteins, and more specifically to the overwhelming tdTomato labeling in the neuropil of densely transduced dorsal horn regions and in the central processes of transduced DRG neurons. The high fluorescence intensity of these regions required imaging parameters that were not optimal for regions with lower density of transduced neurons. In contrast, the discrete nuclear localization of Cre-GFP allowed clear visualization of individual nuclei in the spinal cord. **E and F,** tdTomato (red, subscript 1) and GFP (green, subscript 2) immunofluorescence in neurons of the ipsilateral L4 DRG following transduction with AAV9 (E) or AAV2retro (F); not all tdTomato-labeled cells were immunoreactive for nuclear GFP, scale bars = 150μm. **G and H,** NeuroTrace staining (blue, subscript 1), tdTomato (red, subscript 2) and CGRP (green, subscript 3) immunofluorescence in the ipsilateral L4 DRG following transduction with AAV9 (G) or AAV2retro (H); arrows point to examples of tdTomato and CGRP colocalization, scale bars = 100 μm.

https://doi.org/10.1371/journal.pone.0264938.g002

labeled neurons, a threshold mean gray value was selected for the entire data set based on the rate of change of the slope of the cumulative mean gray value frequency distribution.

Quantitative analysis of DRG neurons after intracolonic delivery

For quantitative analysis of transduction in DRG neurons after intracolonic AAV delivery, native tdTomato and GFP fluorescence was imaged in whole-mounted L6 DRG (without clearing) on a two-photon Nikon A1R system as described above for Fig 4A1 and 4B1. tdTomato or GFP-expressing neurons in the z-stacks were manually counted by an observer blinded to the treatments.

Statistics

The number of animals in each condition was used as the value of n. The distribution of spino-parabrachial neurons within the dorsal spinal cord was compared by two-way ANOVA with Bonferroni corrected post testing for pairwise comparisons (AAV treatment x spinal laminae, data shown in Fig 1 pie charts). Comparisons between ipsilateral and contralateral distributions were made using Fisher's exact test (data shown in Fig 1 stacked columns and pie charts). For intrathecal injections, the relative cumulative distributions of the area of labeled DRG neurons were compared using the Kolmogorov-Smirnov test (Fig 3F). Due to a significant difference between within group variance, comparison of the mean area of DRG neurons was made using Welch's one-way ANOVA with Dunnet's T3 multiple comparisons test. Statistical analysis and graphical representation of data was performed using Prism 9 software with $\alpha = 0.05$.
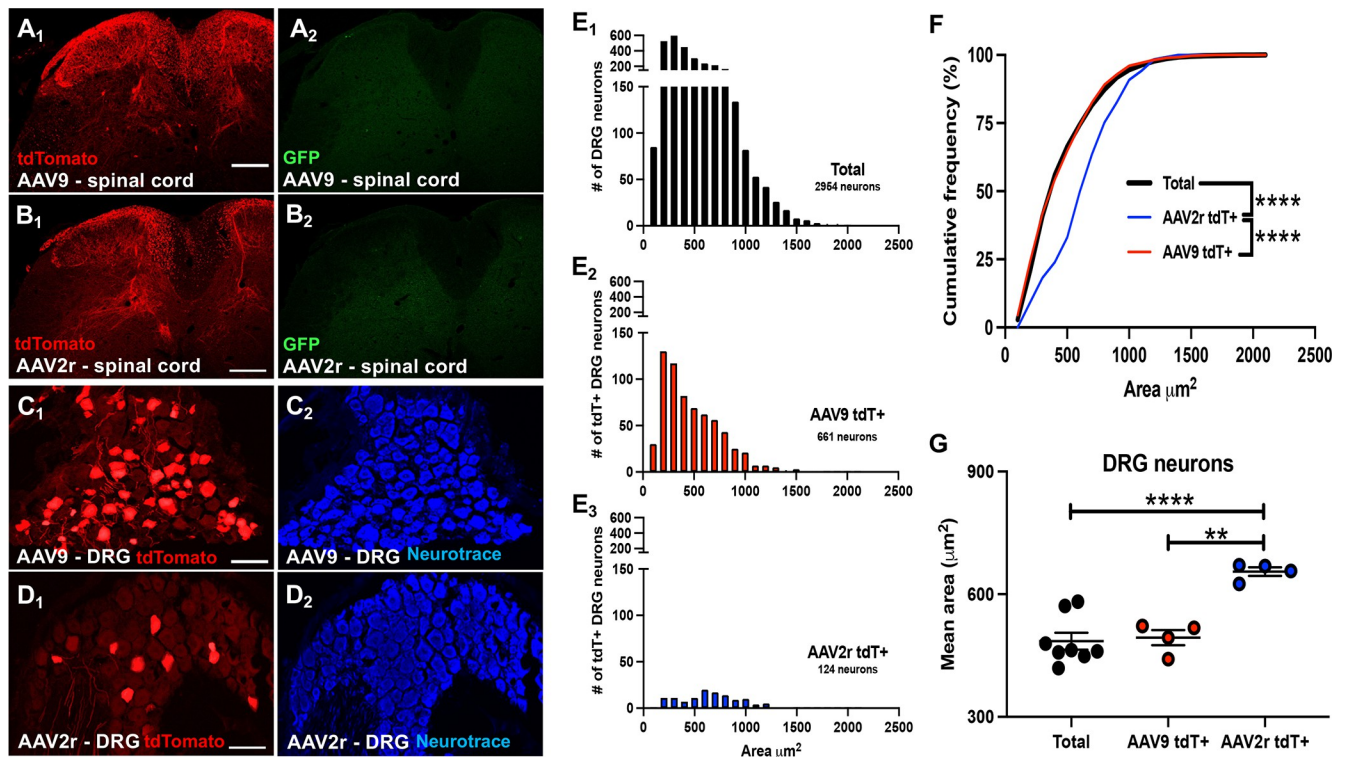
Fig 3. Transduction of spinal cord and DRG neurons following intrathecal delivery of AAV9 and AAV2retro. A and B, tdTomato (red, subscript 1) and GFP (green, subscript 2) immunofluorescence in the lumbar spinal cord of mice injected with AAV9 (A) or AAV2retro (B); scale bars = 200μm. **C and D,** tdTomato (red, subscript 1) immunofluorescence and NeuroTrace staining (blue, subscript 2) showing transduced neurons in L4 DRG following injection of AAV9 (C) or AAV2retro (D); scale bars = 100μm. **E,** NeuroTrace (C2, D2) was used to quantify the area of individual L4 DRG neurons. The areas of total (E1), AAV9 transduced tdTomato+ (E2), and AAV2retro transduced tdTomato+ (E3) DRG neurons are shown as frequency histograms to illustrate the number of DRG neurons relative to their area (μm^2). **F,** The cumulative frequency distribution plot of DRG neuron area shows that while the size distribution of AAV9 tdT+ DRG neurons (red line) closely matches that of total NeuroTrace labeled DRG neurons (black line; Kolmogorov-Smirnov test, p>0.05), the size distribution of the AAV2retro tdT+ DRG neuron population (blue line) is skewed toward larger cells compared to both the total DRG neuron population, and the AAV9 tdT+ DRG neuron population, with 66.35% of the total DRG neuron population and 59.84% of the AAV9 tdT+ DRG neuron population comprised of neurons with an area $\leq 500 \ \mu m^2$, while only 33.06% of the AAV2r+ DRG neuron population has an area $\leq 500 \ \mu m^2$ (Kolmogorov-Smirnov test, **** = p<0.0001). **G,** Each dot represents the mean area of DRG neurons from a single animal (n = animal #). The mean area of AAV2retro tdT+ DRG neurons is significantly larger than the mean area of total, and AAV9 tdT+, DRG neurons (Welch's one-way ANOVA with Dunnet's T3 multiple comparisons test ** = p<0.01; **** = p<0.0001).

https://doi.org/10.1371/journal.pone.0264938.g003

Results

Differential targeting of spinal projection neurons by AAV9 and AAV2retro

To selectively transduce somatosensory projection neurons of the dorsal horn, Ai14 reporter mice were injected in the parabrachial complex with AAV9 (3×10^{13} GC/mL) or AAV2retro (2.5×10^{14} GC/mL) vectors (n = 5 per treatment) expressing GFP-tagged Cre recombinase. To compare viral transduction rates with a retrograde labeling method employed in functional assays, a separate cohort of C57/Bl6 mice (n = 8) was injected with the lipophilic fluorescent dye Fast-DiI. Fig 1 shows examples of parabrachial injection sites and labeled spinal projection neurons in histological sections derived from Ai14 mice injected with AAV9 (Fig 1A), AAV2-retro (Fig 1B), or Fast-DiI (Fig 1C). While these injection sites are consistent with reports quantifying spinoparabrachial neurons [29], we cannot rule out that injectate may have spread to the periaqueductal grey. Therefore, our sample of retrogradely labeled neurons may include parabrachial and periaqueductal grey projecting spinal neurons. Expression of the tdTomato
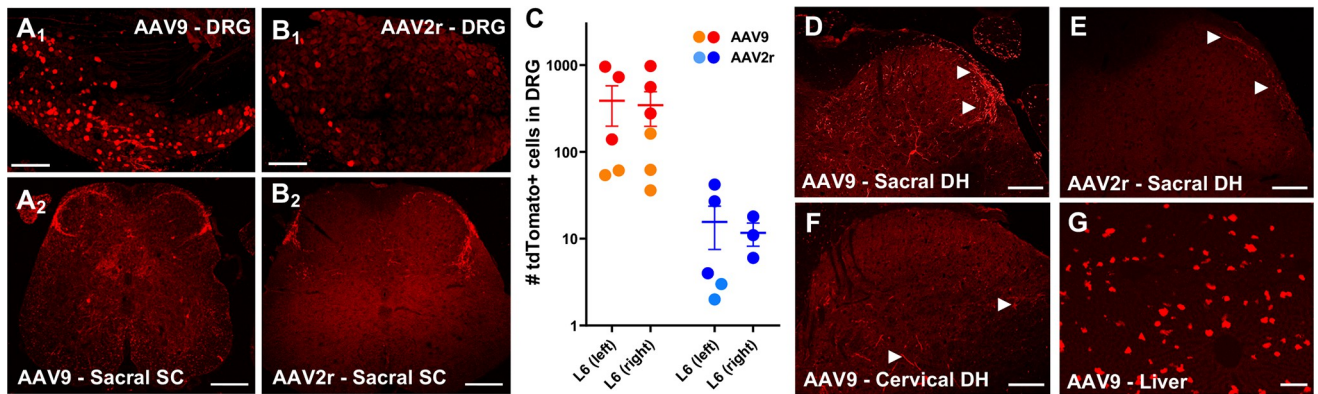
Fig 4. AAV9 and AAV2retro-mediated transduction following intracolonic injections. A and B, tdTomato labeling in L6 DRG and sacral spinal cord was more abundant in AAV9-injected compared to AAV2retro injected animals from cohort 1. The images in A1 and B1 represent a maximum intensity projection of four stitched 3D stacks spanning the entire ganglion (collected with a 3 μm z-step). Scale bars: A1 and B1, 150 μm; A2 and B2, 100 μm. **C,** Quantitative analysis of tdTomato expressing L6 DRG neurons from cohort 1 (circles) and cohort 2 (squares). **D-E,** Sacral spinal cords from cohort 2 showed labelling of afferent fibers and a few neurons in the spinal cord, consistent with the previously observed pattern (D, E). Scale bar = 100μm. **F-G,** The presence of tdTomato labelled fibers and cells in cervical spinal cord as well as cells of the liver provides evidence for systemic distribution of AAV9 (F, G). Scale bars: F, 100μm; G, 150μm.

reporter protein and the viral Cre/GFP was visualized by immunolabeling. Notably, GFP labeling was rarely observed in the tdTomato-positive transduced neurons, suggesting that although sufficient for Cre-dependent recombination, the expression levels of Cre/GFP were below the detection limit of visualization. Ai14 mice without viral injection showed no tdTomato fluorescence in either the brain or the spinal cord (not shown).

The number and location of spinoparabrachial neurons labeled by tdTomato expression or Fast-DiI was quantified in the dorsal horn (DH) and lateral spinal nucleus (LSN) from 30μm transverse sections of the rostral lumbar enlargement (L1-L3). The relative proportions of labeled neurons in the LSN and DH following AAV9 and AAV2retro parabrachial injections was notably different (Fig 1D, stacked bars). Following AAV9 treatment, over 80% of the retrogradely labeled projection neurons were located in DH. In contrast, AAV2retro labeled projection neurons in the DH and LSN equally. These distinct patterns of labeling were observed in spinal cord both ipsilateral and contralateral to the site of parabrachial injection. The distribution of DiI-labeled neurons largely paralleled that of AAV2retro-targeted neurons, although there was a trend toward higher proportions of DiI-labeled neurons within the LSN, particularly on the ipsilateral side.

The lamina I transduction rates expressed as neurons per 1 mm of rostro-caudal spinal cord length contra- and ipsilateral to the injection site respectively were as follows: 2.5 ± 1.3 and 4.6 ± 2.5 for AAV9, compared to 23.5 ± 8.1 and 7.4 ± 3.3 for AAV2retro. The corresponding labeling rate for Fast-DiI was 42.7 ± 16.8 in the contralateral lamina I, and 9.9 ± 3.9 on the ipsilateral side. Although differences in vector titer precluded direct comparison of transduction efficiency between the AAV9 and AAV2retro vectors, we compared the distribution of labeled DH neurons between the treatment groups (Fig 1D, pie charts). The proportion of AAV9 labeled projection neurons found in lamina I of the contralateral DH was significantly lower than that observed with AAV2retro, which showed a pattern similar to Fast-DiI. Furthermore, Fisher's exact testing of the proportion of superficial labeled neurons (lamina I) compared to deep labeled neurons (laminae III-V) revealed a significant difference between ipsilateral and contralateral sides of animals injected with AAV2retro (Fisher's exact test; $p < 0.05$) or Fast-DiI (Fisher's exact test; $p < 0.0001$). This pattern was not observed with AAV9,

which showed no significant difference in the relative distribution of superficial versus deep labeled neurons between the ipsilateral and contralateral side (Fisher's exact test; p>0.05).

AAV2retro was readily transported retrogradely and transduced neurons in numerous distant areas of the brain including cingulate cortex, orbital cortex, primary motor cortex and primary somatosensory cortex. Consistent with the transduction of neurons in primary motor cortex (Fig 1F), we observed prominent labeling of the dorsal corticospinal tract (Fig 1B2, long arrow). In contrast, AAV9-mediated transduction was largely limited to the brainstem and was never seen in cortical regions. The labeling of tracts within the white matter of the spinal cord is summarized in Fig 1E.

AAV9 and AAV2retro vectors effectively transduce spinal dorsal horn and dorsal root ganglion neurons when delivered intraspinally

To assess the utility of AAV9 and AAV2retro in targeting the somatosensory system at the level of the spinal cord, we performed intraspinal injections of the vectors into the lumbar enlargement of Ai14 mice (AAV9, n = 3; AAV2retro, n = 4) and observed viral transduction of neurons in the spinal cord and dorsal root ganglia (DRG). Fig 2 shows representative images of immunolabeling of the tdTomato reporter and the virally expressed Cre-GFP in spinal cord from mice injected with AAV9 (Fig 2A and 2B) or AAV2retro (Fig 2C and 2D). The highest levels of labeling for both tdTomato and GFP were seen in the ipsilateral dorsal horn. In this region, tdTomato labeling was noted both in neuronal somata and in their processes, whereas GFP labeling was localized in neuronal nuclei consistent with the nuclear localization of Cre. tdTomato-expressing neuronal somata were also evident in the L4 DRG ipsilateral to the intraspinal injections of AAV9 (Fig 2E) and AAV2retro (Fig 2F). The level of GFP expression in the DRG as compared to the dorsal horn was consistently lower. Furthermore, the virally expressed GFP was not detected in a large portion of tdTomato-positive DRG neurons. Colocalization of calcitonin-gene-related-peptide (CGRP) immunofluorescence with tdTomato in L4 DRG from Ai14 mice that received intraspinal injection of AAV9 (Fig 2G) or AAV2r (Fig 2H) shows that both vectors can transduce peptidergic primary nociceptors. The proportion of DRG neurons transduced by AAV9 ($8.5x10^{13}$ GC/mL) was quantified in a second cohort of mice (n = 3) and was found to be approximately 21% (range 17–23%). These data confirm that both AAV9 and AAV2retro effectively transduce somatosensory neurons of the dorsal horn and DRG when injected intraspinally. In addition, they highlight the higher sensitivity in detecting AAV transduction based on reporter expression (tdTomato) compared to viral protein expression (Cre/GFP).

AAV9 and AAV2retro vectors transduce DRG neurons following intrathecal delivery

Intrathecal injection offers the least invasive route of viral vector administration to the CNS. Intrathecal delivery of 10 μl of AAV9 ($8.5x10^{13}$ GC/mL, n = 5) or AAV2retro ($1x10^{13}$ GC/mL, n = 6) resulted in prominent tdTomato labeling in spinal dorsal horn (Fig 3A1 and 3B1). Compared to intraspinal viral vector delivery (Fig 2), relatively few spinal neurons were transduced, and the vast majority of tdTomato immunofluorescence present in the spinal cord was localized to the central processes of primary afferent neurons (identified morphologically). This was confirmed by a relative dearth of viral GFP immunofluorescence in spinal cord (Fig 3A2 and 3B2), and expression of tdTomato by transduced DRG neurons (Fig 3C1 and 3D1). Counter staining with NeuroTrace to label all L4 DRG neurons (Fig 3C2 and 3D2) allowed us to estimate the proportions of viral labeled neurons at approximately 54% (range 36–82%) following intrathecal delivery of AAV9, while AAV2retro delivery transduced approximately 6%

(range 0.7–20%). This difference is illustrated in the frequency histograms of Fig 3E. While differences in the viral titers precluded meaningful comparison of the absolute number of transduced neurons, we analyzed the area of the total and AAV transduced DRG neuron populations as measured from NeuroTrace-stained histological sections (Fig 3C2 and 3D2). The frequency distributions for total DRG neurons, AAV9 transduced tdTomato positive (AAV9 tdT+), DRG neurons and AAV2retro transduced tdTomato positive (AAV2r tdT+) DRG neurons are shown in Fig 3E as the number of cells over soma area, and in Fig 3F as a cumulative frequency distribution plot. The cumulative frequency distribution is relative, and thus, allows statistical comparison of soma size distribution despite differences in the number of cells labeled. The relative cumulative soma size distribution for AAV9 tdT+ DRG neurons (Fig 3F, red line) closely follows that of the total DRG neuron population (Fig 3F, black line), suggesting that AAV9 does not exhibit a modality preference in its transduction of primary afferent neurons when delivered intrathecally. Conversely, the relative cumulative soma size distribution for AAV2retro tdT+ DRG neurons (Fig 3F, blue line), is significantly shifted rightward compared to the distribution of total and AAV9 tdT+ DRG neuron populations. This suggests that in our experiments AAV2retro exhibited a preference for transduction of primary afferent DRG neurons with larger soma sizes, which are more likely to be non-nociceptive mechanoreceptors than nociceptors. Group-wise analysis of mean soma size confirms that tdTomato positive L4 DRG neurons transduced by AAV2retro are on average significantly larger than those transduced by AAV9, and larger than the mean soma size of the total DRG neuron population (Fig 3G).

AAV9- and AAV2retro transduce DRG neurons differentially via their peripheral processes

To determine whether AAV9 and AAV2retro transduce primary afferent neurons via their peripheral processes, we examined transduction in DRG following delivery of the vectors into the wall of the descending colon. In the mouse, the sensory innervation of the descending colon is provided predominantly by L5, L6, and S1 DRG [30]. Transduction was evaluated based on detection of native tdTomato and GFP fluorescence within DRG neurons in whole-mount preparations of L6 DRG from Ai14 mice injected with AAV9 or AAV2retro vectors driving expression of Cre-GFP. A single intracolonic injection of AAV9 (2.7×10^{13} GC/mL) yielded a higher number of tdTomato-expressing DRG neurons than an injection of AAV2retro (2.5×10^{14} GC/mL), indicating that AAV9 transduces DRG neurons more effectively than AAV2retro via this route of delivery (Fig 4A1, 4B1 and 4C). Strikingly, GFP fluorescence was not observed in AAV9- or AAV2retro DRG (not shown). To test whether the lack of native GFP fluorescence was entirely attributable to a detection limit in the whole-mount preparations, we examined DRG transduction with the same AAV9 vector in two wild-type C57/Bl6 mice. Counting of labeled cells in two L6 DRG from these mice yielded 132 and 55 GFP-positive neurons, respectively. These results suggest that viral expression of Cre/GFP in DRG neurons may be suppressed following Cre-dependent recombination in Ai14 mice.

   At lower lumbar and sacral spinal cord levels, both AAV9 and AAV2retro intracolonic treatments in Ai14 mice resulted in tdTomato labeling of nerve fibers in superficial dorsal horn and to a lesser extent in the intermediate gray matter (Fig 4A2, 4B2, 4D and 4E). Surprisingly, we also observed scattered labeling of neurons within the spinal cords of AAV9-treated mice (Fig 4A2 and 4D). While some of these neurons could be preganglionic parasympathetic neurons projecting to the colon, it is also possible that the labeling of spinal neurons is due to trans-synaptic transfer of AAV9 [31] or to access of AAV9 to the systemic circulation following intracolonic delivery. To address the latter possibility, we treated a second cohort of mice

with a different set of AAV9 (8.5×10^{13} GC/mL) or AAV2retro (1×10^{13}GC/mL) vectors (same as used for intrathecal injections) and extended the histological analysis to cervical spinal cord (Fig 4F) and liver (Fig 4G). The superior level of transduction achieved by AAV9 was consistent between the two cohorts (Fig 4C). In lower lumbar and sacral spinal cord, we observed labeling for both vectors in a pattern similar to the first cohort. In contrast, in cervical spinal cord, tdTomato labeling was observed in AAV9- (Fig 4F) but not AAV2retro-treated (not shown) mice. Unlike lower lumbar and sacral levels (Fig 4A2), the pattern of AAV9-mediated tdTomato expression in cervical spinal cord consisted of scattered fibers and few neurons without prominent labeling of fibers in superficial dorsal horn (Fig 4F). Transduction was also noted in the liver of AAV9- (Fig 4G) but not AAV2retro-treated (not shown) mice following intracolonic delivery. The presence of AAV9-mediated transduction in cervical spinal cord and liver suggests that AAV9 gains access to the systemic circulation following intracolonic delivery.

Discussion

In the present study, we characterized the ability of AAV2retro and AAV9 to transduce components of the somatosensory system via different routes of delivery. Our results indicate notable differences in the access of the two AAV serotypes to primary afferent neurons via peripheral delivery and to spinal projection neurons via intracranial delivery within the parabrachial complex. These differences likely result from mechanisms that govern the diverse cellular tropism of AAV serotypes and remain poorly understood [32]. AAV9 and AAV2 (the parent serotype of AAV2retro) bind to different primary and secondary receptors on the cell surface [32]. AAV9 is distinguished from other serotypes by its more efficient systemic distribution to various tissues and organs and its ability to cross the blood-brain barrier [1, 33]. On the other hand, AAV2retro harbors engineered capsid mutations that, through unknown mechanisms, confer enhanced transduction efficiency via retrograde transport [21].

We evaluated neuronal transduction based on Cre-dependent expression of tdTomato, controlled by the CAG promoter, following delivery of AAV9 or AAV2retro carrying identical constructs that drive the expression of Cre/GFP, under the control of the hSyn promoter. Surprisingly, we observed a number of instances of non-overlapping tdTomato and Cre/GFP labeling. In spinal neurons transduced via intraspinal delivery the apparent discrepancy in tdTomato and Cre/GFP labeling was largely due to the different subcellular localization of the two transgenes and the overwhelming intensity of tdTomato labeling as outlined in the legend of Fig 2. We also observed multiple instances of spinal projection neurons and DRG neurons that were tdTomato-positive but lacked Cre/GFP labeling, indicating that Cre/GFP expression levels were sufficient for Cre-recombination but below the detection limit for immunohistochemical detection. The discrepancy in tdTomato and Cre/GFP labeling in these neurons may reflect entry of fewer viral particles and the fact the CAG promoter is substantially stronger than the hSyn promoter. These observations highlight the superior sensitivity of detection of neuronal transduction based on reporter expression (i.e. tdTomato) relative to expression of viral products (i.e. Cre/GFP). Limitations in the histological detection of viral transgene expression may affect data interpretation and the assessment of off-target effects in functional studies. Finally, our analysis of Cre/GFP labeling following intracolonic injections in Ai14 and wild-type mice suggests potential suppression of Cre/GFP expression in DRG neurons following Cre-dependent recombination in Ai14 mice. We are not aware of previous reports of similar observations, and the potential underlining mechanisms are unclear. In future studies, it is important to determine whether this phenomenon extends to other mouse reporter lines.

Transduction of spinal projection neurons

The spinal dorsal horn functions as the initial site of integration between sensory information emanating from peripheral tissues and descending modulation from supraspinal levels. Spinal projection neurons constitute only 1% of neurons in the dorsal horn and serve as the output of this integrative circuit. Projection neurons located in superficial lamina I tend to display a high threshold "nociceptive specific" phenotype. In rodents, the vast majority of these nociceptive-specific projection neurons project to the parabrachial nucleus in the midbrain [29]. We targeted these cells for genetic manipulation with viral vectors to aid future investigation into their function and connectivity.

We used the lipophilic dye Fast-DiI as a "universal" retrograde tracer of spinal projection neurons. Although Fast-DiI has been employed for the identification of spinoparabrachial neurons in functional studies [34–36], to our knowledge, the spinal distribution of labeled neurons has not been evaluated histologically in the mouse. Previous neuroanatomical analysis of spinopara-brachial neurons in the mouse was conducted using the retrograde tracer cholera toxin B (CTB) [29]. This study reported an approximately 3-fold higher number of retrogradely labeled neurons at the L4 spinal level than the number of Fast-DiI neurons we observed within the rostral (L1-L3) lumbar spinal cord. This difference in the rate of labeling of projection neurons may be due to the use of different retrograde tracers and the distinct spinal locations of the analyses.

Comparison of the distribution of spinal projection neurons labeled by Fast-DiI, AAV2retro and AAV9 suggests marked differences. Most notably, Fast-DiI was more likely to label projection neurons in the LSN than the AAV vectors. The observation of LSN spinal projection neurons here is consistent with recent identification of a sustained pain coping pathway involving LSN neurons that project to the parabrachial nucleus in the mouse [37]. Our results suggest that AAV9 and AAV2retro may exhibit lower tropism for LSN compared to dorsal horn projection neurons.

Treatment with both AAV2retro and Fast-DiI yielded more labeled neurons in lamina I of the contralateral than the ipsilateral dorsal horn. This is consistent with reports showing that the majority of lamina I spinoparabrachial neurons project to the contralateral midbrain. However, this pattern of labeling was not seen following AAV9 treatment. While we expect that the projection neurons transduced by AAV9 are a subset of the DiI-labeled neurons, our observations suggest that under our experimental conditions AAV9 may target preferentially projection neurons located in deeper laminae. Therefore, the different pattern of transduction of projection neurons by AAV9 and AAV2retro may reflect differential tropism of the two serotypes for different subsets of projection neurons.

Our observations of retrograde transport of AAV9 are consistent with other published work [17, 38, 39]. Interestingly, recent studies have reported that lamina I spinoparabrachial neurons were efficiently transduced by parabrachial complex injection of AAV9, driving expression of transgenes under the control of the strong universal promoters CAG and CB7 [38, 39]. The difference in the strength of these promoters and the hSyn promoter likely accounts for the difference between these observations and our results, consistent with a previous report [17].

Transduction of dorsal horn and DRG neurons following intrathecal and intraspinal AAV delivery

Transduction of dorsal horn neurons by several AAV serotypes delivered intraspinally has been previously described [17]. Our observations of extensive transduction of dorsal horn neurons by AAV9 are consistent with these findings. We also observed abundant spinal transgene

expression in AAV2retro-treated mice, which was qualitatively similar to AAV9-driven expression. Haenraets at al. (2017) demonstrated that, when transgene expression was controlled by the CAG promoter, AAV serotypes 1, 6, 7, 8, 9, and 10 displayed similar transduction efficiencies in dorsal horn targeting more than 70% of excitatory and inhibitory neurons [17]. The exception among the serotypes evaluated in this report was AAV5, which transduced 60% of excitatory and 50% of inhibitory neurons. Given the heterogeneity of dorsal horn neurons [40–42], evaluation of the subtypes of spinal neurons transduced by AAV9 and AAV2retro was beyond the scope of the present study. However, it is possible that the use of a weaker promoter and/or reduced viral load would reveal differential tropism. Surprisingly, there is evidence that the hSyn promoter, which is considered to be pan-neuronal, does not drive expression in a subset of dorsal horn neurons [11]. In contrast to intraspinal delivery, we observed limited transduction of dorsal horn neurons via intrathecal delivery; this observation is consistent with previous reports for AAV9 and other serotypes carrying single-stranded viral constructs [1, 2, 43].

We found that both AAV9 and AAV2retro transduced DRG neurons following intraspinal and intrathecal delivery, although differences in viral titers precluded precise quantitative comparisons of transduction efficiency. Considering several methodological differences, the transduction efficiency we observed for intraspinally delivered AAV9 (~21% of L4 DRG neurons) is consistent with the findings of Haenraets et al. (2017). Furthermore, colocalization with CGRP, a marker of peptidergic nociceptive neurons, suggests that both nociceptive and non-nociceptive neurons are targeted under our experimental conditions. Importantly, Haenraets et al. (2017) demonstrated that a lower AAV9 viral load preferentially targeted DRG neurons expressing CGRP and the marker of myelinated neurons NF200 but not neurons labeled by the non-peptidergic nociceptive marker IB4; this targeting bias was overcome by increasing the viral load. A similar bias observed with the hSyn promoter was also overcome by increasing the viral load. Although comprehensive analysis of DRG neuronal subtypes were outside the scope of our study, these prior observations illustrate the complex relationship between viral load and promoter strength, which should be considered in the design and interpretation of experiments employing AAV for neuronal gene transfer.

Our analysis of the size distribution of DRG neurons transduced by intrathecal delivery of AAV9 and AAV2retro also suggested targeting of both nociceptive (generally, small-diameter) and non-nociceptive neurons (generally, large diameter) and revealed a preference for larger neurons by AAV2retro. However, as discussed above, this preference could be dependent on the promoter and the viral load. It should be noted that the minimally invasive intrathecal injection of AAV9 transduced a higher proportion of L4 DRG neurons (54%, range 36–82%) than intraspinal, but the dose administered intrathecally was higher. In addition, while DRG transduction following intraspinal viral delivery is likely restricted to several segments, transduction via intrathecal delivery is more broadly distributed [1, 44]. Thus, the two routes of administration offer a number of advantages and disadvantages that can be tailored to specific experimental requirements.

Transduction of DRG following intracolonic delivery of AAV

Our observations indicate that AAV9 transduces DRG neurons more efficiently than AAV2retro following intracolonic injection and that AAV9 also appears to gain access to the systemic circulation. The latter conclusion is based on the presence of tdTomato labeling in liver and cervical spinal cord. However, the distinct pattern of labeling in superficial lumbosacral and cervical dorsal horn of AAV9-injected mice suggests that systemic redistribution of the virus accounts for only a small portion of the transduction observed in L6 DRG. Delivery of lower

injection volumes in the periphery may reduce systemic redistribution of AAV9 and improve the selective targeting of neurons innervating the injection site. The extent of transduction due to access of AAV9 to the systemic circulation may also be sex dependent as there is evidence for differential transduction of CNS and liver of male and female mice following intravenous AAV9 delivery [45, 46]. Finally, it remains to be determined whether intracolonic delivery of AAV9 leads to transduction of preganglionic parasympathetic neurons or trans-synaptic anterograde gene transfer to spinal neurons in lower lumbar and sacral spinal cord.

We observed that AAV2retro intracolonic injection yielded a substantially lower number of transduced DRG neurons, regardless of titer differences of the viral preparations. This suggests that the determinants that confer enhanced transduction efficiency of AAV2retro via retrograde transport in the CNS are not present in the peripheral processes of DRG neurons innervating the distal colon. It is unclear if other peripheral DRG targets would display similar characteristics. However, since AAV2retro-mediated transduction remained limited to the injection site, this serotype may be useful for selective organ-specific targeting of DRG neurons in paradigms where a relatively lower rate of transduction is acceptable.

Limitations

Several factors that may affect the distribution and/or detection of gene transfer, such as different promoters [17] and survival times, were not examined here, Moreover, different preparations of the same vector may vary substantially [47]. Further investigation of these factors is needed to optimize targeting depending on experimental need.

Conclusions

The results of the present study characterize the utility of AAV9 and AAV2retro for gene transfer to different components of the somatosensory system. The use of a reporter mouse line allowed for high sensitivity in the assessment of transgene expression and the biodistribution of the viral vectors. Our results suggest differential tropism of AAV9 and AAV2retro for spinal projection neurons. In addition, we observed differences in the targeting of primary afferent neurons via peripheral administration of the viral vector. These observations can assist in tailoring the application of AAV9 and AAV2retro in studies of the somatosensory system. While in our experiments both nociceptive and non-nociceptive neurons were targeted in the dorsal horn and DRG, the use of appropriate Cre-lines (for example, NaV1.8-cre [48]) in combination with Cre-dependent AAV vectors can achieve selectivity in targeting functional subtypes of somatosensory neurons.

Acknowledgments

Author Contributions

Conceptualization: Lucy Vulchanova.

Formal analysis: Alexander G. J. Skorput, Reshma Gore.

Funding acquisition: Lucy Vulchanova.

Investigation: Alexander G. J. Skorput, Reshma Gore, Rachel Schorn, Maureen S. Riedl, Bailey Hadlich, Kelley F. Kitto.

Project administration: Lucy Vulchanova.

Resources: Ezequiel Marron Fernandez de Velasco.

Supervision: Maureen S. Riedl, Carolyn A. Fairbanks, Lucy Vulchanova.

Validation: Alexander G. J. Skorput, Reshma Gore, Lucy Vulchanova.

Visualization: Alexander G. J. Skorput, Reshma Gore, Lucy Vulchanova.

Writing – original draft: Alexander G. J. Skorput, Lucy Vulchanova.

Writing – review & editing: Alexander G. J. Skorput, Reshma Gore, Maureen S. Riedl, Ezequiel Marron Fernandez de Velasco, Carolyn A. Fairbanks, Lucy Vulchanova.

References

1. Schuster DJ, Dykstra JA, Riedl MS, Kitto KF, Belur LR, McIvor RS, et al. Biodistribution of adeno-associated virus serotype 9 (AAV9) vector after intrathecal and intravenous delivery in mouse. Frontiers in neuroanatomy. 2014; 8:42. https://doi.org/10.3389/fnana.2014.00042 PMID: 24959122; PubMed Central PMCID: PMC4051274.

2. Vulchanova L, Schuster DJ, Belur LR, Riedl MS, Podetz-Pedersen KM, Kitto KF, et al. Differential adeno-associated virus mediated gene transfer to sensory neurons following intrathecal delivery by direct lumbar puncture. Molecular pain. 2010; 6:31. Epub 2010/06/01. https://doi.org/10.1186/1744-8069-6-31 PMID: 20509925; PubMed Central PMCID: PMC2900238.

3. Gallaher ZR, Steward O. Modest enhancement of sensory axon regeneration in the sciatic nerve with conditional co-deletion of PTEN and SOCS3 in the dorsal root ganglia of adult mice. Experimental neurology. 2018; 303:120–33. Epub 2018/02/20. https://doi.org/10.1016/j.expneurol.2018.02.012 PMID: 29458059; PubMed Central PMCID: PMC5864562.

4. Yu H, Fischer G, Hogan QH. AAV-Mediated Gene Transfer to Dorsal Root Ganglion. Methods Mol Biol. 2016; 1382:251–61. Epub 2015/11/28. https://doi.org/10.1007/978-1-4939-3271-9_18 PMID: 26611592; PubMed Central PMCID: PMC5459312.

5. Zhang Z, Zheng B, Du S, Han G, Zhao H, Wu S, et al. Eukaryotic initiation factor 4 gamma 2 contributes to neuropathic pain through downregulation of Kv1.2 and the mu opioid receptor in mouse primary sensory neurones. Br J Anaesth. 2020. Epub 2020/12/12. https://doi.org/10.1016/j.bja.2020.10.032 PMID: 33303185

6. Iyer SM, Montgomery KL, Towne C, Lee SY, Ramakrishnan C, Deisseroth K, et al. Virally mediated optogenetic excitation and inhibition of pain in freely moving nontransgenic mice. Nat Biotechnol. 2014; 32(3):274–8. Epub 2014/02/18. https://doi.org/10.1038/nbt.2834 PMID: 24531797; PubMed Central PMCID: PMC3988230.

7. Towne C, Pertin M, Beggah AT, Aebischer P, Decosterd I. Recombinant adeno-associated virus serotype 6 (rAAV2/6)-mediated gene transfer to nociceptive neurons through different routes of delivery. Mol Pain. 2009; 5:52. https://doi.org/10.1186/1744-8069-5-52 PMID: 19737386.

8. Bloom DC, Watson ZL, Neumann DM. Peripheral AAV Injection for Retrograde Transduction of Dorsal Root and Trigeminal Ganglia. Methods Mol Biol. 2019; 1950:237–47. Epub 2019/02/21. https://doi.org/10.1007/978-1-4939-9139-6_13 PMID: 30783977.

9. Watson ZL, Ertel MK, Lewin AS, Tuli SS, Schultz GS, Neumann DM, et al. Adeno-associated Virus Vectors Efficiently Transduce Mouse and Rabbit Sensory Neurons Coinfected with Herpes Simplex Virus 1 following Peripheral Inoculation. J Virol. 2016; 90(17):7894–901. Epub 2016/06/24. https://doi.org/10.1128/JVI.01028-16 PMID: 27334582; PubMed Central PMCID: PMC4988153.

10. Dickie AC, Bell AM, Iwagaki N, Polgar E, Gutierrez-Mecinas M, Kelly R, et al. Morphological and functional properties distinguish the substance P and gastrin-releasing peptide subsets of excitatory interneuron in the spinal cord dorsal horn. Pain. 2019; 160(2):442–62. Epub 2018/09/25. https://doi.org/10.1097/j.pain.0000000000001406 PMID: 30247267; PubMed Central PMCID: PMC6330098.

11. Peirs C, Williams SG, Zhao X, Arokiaraj CM, Ferreira DW, Noh MC, et al. Mechanical Allodynia Circuitry in the Dorsal Horn Is Defined by the Nature of the Injury. Neuron. 2021; 109(1):73–90 e7. Epub 2020/11/13. https://doi.org/10.1016/j.neuron.2020.10.027 PMID: 33181066; PubMed Central PMCID: PMC7806207.

12. Petitjean H, Bourojeni FB, Tsao D, Davidova A, Sotocinal SG, Mogil JS, et al. Recruitment of Spinopar-abrachial Neurons by Dorsal Horn Calretinin Neurons. Cell Rep. 2019; 28(6):1429–38 e4. Epub 2019/08/08. https://doi.org/10.1016/j.celrep.2019.07.048 PMID: 31390558.

13. Chen Q, Roeder Z, Li MH, Zhang Y, Ingram SL, Heinricher MM. Optogenetic Evidence for a Direct Circuit Linking Nociceptive Transmission through the Parabrachial Complex with Pain-Modulating Neurons of the Rostral Ventromedial Medulla (RVM). eNeuro. 2017; 4(3). Epub 2017/07/01. https://doi.org/10.1523/ENEURO.0202-17.2017 PMID: 28660248; PubMed Central PMCID: PMC5483601.

14. Chiang MC, Nguyen EK, Canto-Bustos M, Papale AE, Oswald AM, Ross SE. Divergent Neural Pathways Emanating from the Lateral Parabrachial Nucleus Mediate Distinct Components of the Pain Response. Neuron. 2020; 106(6):927–39 e5. Epub 2020/04/15. https://doi.org/10.1016/j.neuron.2020.03.014 PMID: 32289251.

15. Francois A, Low SA, Sypek EI, Christensen AJ, Sotoudeh C, Beier KT, et al. A Brainstem-Spinal Cord Inhibitory Circuit for Mechanical Pain Modulation by GABA and Enkephalins. Neuron. 2017; 93(4):822–39 e6. Epub 2017/02/07. https://doi.org/10.1016/j.neuron.2017.01.008 PMID: 28162807; PubMed Central PMCID: PMC7354674.

16. Hua T, Chen B, Lu D, Sakurai K, Zhao S, Han BX, et al. General anesthetics activate a potent central pain-suppression circuit in the amygdala. Nat Neurosci. 2020; 23(7):854–68. Epub 2020/05/20. https://doi.org/10.1038/s41593-020-0632-8 PMID: 32424286; PubMed Central PMCID: PMC7329612.

17. Haenraets K, Foster E, Johannssen H, Kandra V, Frezel N, Steffen T, et al. Spinal nociceptive circuit analysis with recombinant adeno-associated viruses: the impact of serotypes and promoters. J Neurochem. 2017; 142(5):721–33. Epub 2017/07/13. https://doi.org/10.1111/jnc.14124 PMID: 28700081.

18. Mason MR, Ehlert EM, Eggers R, Pool CW, Hermening S, Huseinovic A, et al. Comparison of AAV serotypes for gene delivery to dorsal root ganglion neurons. Mol Ther. 2010; 18(4):715–24. Epub 2010/02/25. https://doi.org/10.1038/mt.2010.19 PMID: 20179682; PubMed Central PMCID: PMC2862541.

19. Elmallah MK, Falk DJ, Nayak S, Federico RA, Sandhu MS, Poirier A, et al. Sustained correction of motoneuron histopathology following intramuscular delivery of AAV in pompe mice. Mol Ther. 2014; 22(4):702–12. Epub 2013/12/18. https://doi.org/10.1038/mt.2013.282 PMID: 24336173; PubMed Central PMCID: PMC3982493.

20. Murlidharan G, Samulski RJ, Asokan A. Biology of adeno-associated viral vectors in the central nervous system. Frontiers in molecular neuroscience. 2014; 7:76. Epub 2014/10/07. https://doi.org/10.3389/fnmol.2014.00076 PMID: 25285067; PubMed Central PMCID: PMC4168676.

21. Tervo DG, Hwang BY, Viswanathan S, Gaj T, Lavzin M, Ritola KD, et al. A Designer AAV Variant Permits Efficient Retrograde Access to Projection Neurons. Neuron. 2016; 92(2):372–82. Epub 2016/10/21. https://doi.org/10.1016/j.neuron.2016.09.021 PMID: 27720486; PubMed Central PMCID: PMC5872824.

22. Choi S, Hachisuka J, Brett MA, Magee AR, Omori Y, Iqbal NU, et al. Parallel ascending spinal pathways for affective touch and pain. Nature. 2020; 587(7833):258–63. Epub 2020/10/30. https://doi.org/10.1038/s41586-020-2860-1 PMID: 33116307; PubMed Central PMCID: PMC7666110.

23. Condylis C, Lowet E, Ni J, Bistrong K, Ouellette T, Josephs N, et al. Context-Dependent Sensory Processing across Primary and Secondary Somatosensory Cortex. Neuron. 2020; 106(3):515–25 e5. Epub 2020/03/14. https://doi.org/10.1016/j.neuron.2020.02.004 PMID: 32164873; PubMed Central PMCID: PMC7210055.

24. Kayyal H, Yiannakas A, Kolatt Chandran S, Khamaisy M, Sharma V, Rosenblum K. Activity of Insula to Basolateral Amygdala Projecting Neurons is Necessary and Sufficient for Taste Valence Representation. J Neurosci. 2019; 39(47):9369–82. Epub 2019/10/11. https://doi.org/10.1523/JNEUROSCI.0752-19.2019 PMID: 31597726; PubMed Central PMCID: PMC6867822.

25. Phillips JW, Schulmann A, Hara E, Winnubst J, Liu C, Valakh V, et al. A repeated molecular architecture across thalamic pathways. Nat Neurosci. 2019; 22(11):1925–35. Epub 2019/09/19. https://doi.org/10.1038/s41593-019-0483-3 PMID: 31527803; PubMed Central PMCID: PMC6819258.

26. Fairbanks CA. Spinal delivery of analgesics in experimental models of pain and analgesia. Adv Drug Deliv Rev. 2003; 55(8):1007–41. Epub 2003/08/26. https://doi.org/10.1016/s0169-409x(03)00101-7 PMID: 12935942.

27. Hylden JL, Wilcox GL. Intrathecal substance P elicits a caudally-directed biting and scratching behavior in mice. Brain Res. 1981; 217(1):212–5. https://doi.org/10.1016/0006-8993(81)90203-1 PMID: 6167328

28. Gore R, Riedl MS, Kitto KF, Fairbanks CA, Vulchanova L. AAV-Mediated Gene Delivery to the Enteric Nervous System by Intracolonic Injection. Methods Mol Biol. 2019; 1950:407–15. Epub 2019/02/21. https://doi.org/10.1007/978-1-4939-9139-6_24 PMID: 30783988; PubMed Central PMCID: PMC7241593.

29. Cameron D, Polgar E, Gutierrez-Mecinas M, Gomez-Lima M, Watanabe M, Todd AJ. The organisation of spinoparabrachial neurons in the mouse. Pain. 2015; 156(10):2061–71. Epub 2015/06/24. https://doi.org/10.1097/j.pain.0000000000000270 PMID: 26101837; PubMed Central PMCID: PMC4770364.

30. Christianson JA, Traub RJ, Davis BM. Differences in spinal distribution and neurochemical phenotype of colonic afferents in mouse and rat. J Comp Neurol. 2006; 494(2):246–59. https://doi.org/10.1002/cne.20816 PMID: 16320237.

31. Zingg B, Chou XL, Zhang ZG, Mesik L, Liang F, Tao HW, et al. AAV-Mediated Anterograde Transsynaptic Tagging: Mapping Corticocollicular Input-Defined Neural Pathways for Defense Behaviors. Neuron. 2017; 93(1):33–47. Epub 2016/12/19. https://doi.org/10.1016/j.neuron.2016.11.045 PMID: 27989459; PubMed Central PMCID: PMC5538794.

32. Dhungel BP, Bailey CG, Rasko JEJ. Journey to the Center of the Cell: Tracing the Path of AAV Transduction. Trends Mol Med. 2021; 27(2):172–84. Epub 2020/10/20. https://doi.org/10.1016/j.molmed.2020.09.010 PMID: 33071047.

33. Zincarelli C, Soltys S, Rengo G, Rabinowitz JE. Analysis of AAV serotypes 1–9 mediated gene expression and tropism in mice after systemic injection. Mol Ther. 2008; 16(6):1073–80. Epub 2008/04/17. https://doi.org/10.1038/mt.2008.76 PMID: 18414476.

34. Brewer CL, Li J, O'Conor K, Serafin EK, Baccei ML. Neonatal Injury Evokes Persistent Deficits in Dynorphin Inhibitory Circuits within the Adult Mouse Superficial Dorsal Horn. J Neurosci. 2020; 40(20):3882–95. Epub 2020/04/16. https://doi.org/10.1523/JNEUROSCI.0029-20.2020 PMID: 32291327; PubMed Central PMCID: PMC7219299.

35. Hachisuka J, Baumbauer KM, Omori Y, Snyder LM, Koerber HR, Ross SE. Semi-intact ex vivo approach to investigate spinal somatosensory circuits. Elife. 2016; 5. Epub 2016/12/20. https://doi.org/10.7554/eLife.22866 PMID: 27991851; PubMed Central PMCID: PMC5214752.

36. Hachisuka J, Koerber HR, Ross SE. Selective-cold output through a distinct subset of lamina I spinoparabrachial neurons. Pain. 2020; 161(1):185–94. Epub 2019/10/03. https://doi.org/10.1097/j.pain.0000000000001710 PMID: 31577643.

37. Huang T, Lin SH, Malewicz NM, Zhang Y, Zhang Y, Goulding M, et al. Identifying the pathways required for coping behaviours associated with sustained pain. Nature. 2019; 565(7737):86–90. Epub 2018/12/12. https://doi.org/10.1038/s41586-018-0793-8 PMID: 30532001; PubMed Central PMCID: PMC6461409.

38. Browne TJ, Smith KM, Gradwell MA, Iredale JA, Dayas CV, Callister RJ, et al. Spinoparabrachial projection neurons form distinct classes in the mouse dorsal horn. Pain. 2021; 162(7):1977–94. Epub 2021/03/30. https://doi.org/10.1097/j.pain.0000000000002194 PMID: 33779126; PubMed Central PMCID: PMC8208100.

39. Chisholm KI, Lo Re L, Polgar E, Gutierrez-Mecinas M, Todd AJ, McMahon SB. The encoding of cutaneous stimuli by lamina I projection neurons. Pain. 2021. Epub 2021/03/27. https://doi.org/10.1097/j.pain.0000000000002226 PMID: 33769365

40. Haring M, Zeisel A, Hochgerner H, Rinwa P, Jakobsson JET, Lonnerberg P, et al. Neuronal atlas of the dorsal horn defines its architecture and links sensory input to transcriptional cell types. Nat Neurosci. 2018; 21(6):869–80. https://doi.org/10.1038/s41593-018-0141-1 PMID: 29686262.

41. Sathyamurthy A, Johnson KR, Matson KJE, Dobrott CI, Li L, Ryba AR, et al. Massively Parallel Single Nucleus Transcriptional Profiling Defines Spinal Cord Neurons and Their Activity during Behavior. Cell Rep. 2018; 22(8):2216–25. https://doi.org/10.1016/j.celrep.2018.02.003 PMID: 29466745.

42. Todd AJ. Identifying functional populations among the interneurons in laminae I-III of the spinal dorsal horn. Mol Pain. 2017; 13:1744806917693003. https://doi.org/10.1177/1744806917693003 PMID: 28326935; PubMed Central PMCID: PMC5315367.

43. Bey K, Ciron C, Dubreil L, Deniaud J, Ledevin M, Cristini J, et al. Efficient CNS targeting in adult mice by intrathecal infusion of single-stranded AAV9-GFP for gene therapy of neurological disorders. Gene Ther. 2017; 24(5):325–32. Epub 2017/04/21. https://doi.org/10.1038/gt.2017.18 PMID: 28425480.

44. Schuster DJ, Belur LR, Riedl MS, Schnell SA, Podetz-Pedersen KM, Kitto KF, et al. Supraspinal gene transfer by intrathecal adeno-associated virus serotype 5. Frontiers in neuroanatomy. 2014; 8:66. https://doi.org/10.3389/fnana.2014.00066 PMID: 25147505; PubMed Central PMCID: PMC4122912.

45. Maguire CA, Crommentuijn MH, Mu D, Hudry E, Serrano-Pozo A, Hyman BT, et al. Mouse gender influences brain transduction by intravascularly administered AAV9. Mol Ther. 2013; 21(8):1470–1. Epub 2013/08/02. https://doi.org/10.1038/mt.2013.95 PMID: 23903572; PubMed Central PMCID: PMC3734655.

46. Weismann CM, Ferreira J, Keeler AM, Su Q, Qui L, Shaffer SA, et al. Systemic AAV9 gene transfer in adult GM1 gangliosidosis mice reduces lysosomal storage in CNS and extends lifespan. Hum Mol Genet. 2015; 24(15):4353–64. Epub 2015/05/13. https://doi.org/10.1093/hmg/ddv168 PMID: 25964428; PubMed Central PMCID: PMC4492398.

47. O'Connor DM, Lutomski C, Jarrold MF, Boulis NM, Donsante A. Lot-to-Lot Variation in Adeno-Associated Virus Serotype 9 (AAV9) Preparations. Hum Gene Ther Methods. 2019; 30(6):214–25. Epub 2019/11/23. https://doi.org/10.1089/hgtb.2019.105 PMID: 31752530; PubMed Central PMCID: PMC6919242.

48. Daou I, Tuttle AH, Longo G, Wieskopf JS, Bonin RP, Ase AR, et al. Remote optogenetic activation and sensitization of pain pathways in freely moving mice. J Neurosci. 2013; 33(47):18631–40. Epub 2013/11/22. https://doi.org/10.1523/JNEUROSCI.2424-13.2013 PMID: 24259584.